1521-009X/49/3/179–187$35.00
DRUG METABOLISM AND DISPOSITION

https://doi.org/10.1124/dmd.120.000274
Drug Metab Dispos 49:179–187, March 2021

Tryptophan-75 Is a Low-Energy Channel-Gating Residue that Facilitates Substrate Egress/Access in Cytochrome P450 2D6 [S]

Kevin D. McCarty, Samuel A. Ratliff, Kyle A. Furge, and Laura Lowe Furge

Department of Chemistry, Kalamazoo College, Kalamazoo, Michigan

Received October 5, 2020; accepted December 21, 2020

ABSTRACT

CYP2D6 is a major drug metabolizing enzyme with a buried active site. Channels leading to the active site from various enzyme surfaces are believed to facilitate ligand egress and access to the active site. The present study used molecular dynamics (MD) and in vitro studies with CYP2D6*1 and a Trp75-to-Ala mutant to examine channel gating in CYP2D6 by Trp75. MD simulations measured energy landscapes of Trp75 conformations and simulated substrate passage within channel 2b using bufuralol as a model substrate. Trp75 alternated between multiple stable states that supported substrate transport along channel 2b with low-energy barriers between states (~ −1 kcal/mol). Trp75 conformations were stabilized primarily by hydrogen bonding between Trp75 and Glu222, Asn226, Ala225, or Gln72. Energy barriers were low between Trp75 conformations, allowing Trp75 to easily move between various conformations over time and to function in both binding to and moving substrates in the 2b channel of CYP2D6. Michaelis-Menten kinetic studies completed with purified enzyme in a reconstituted system showed overall reduced enzyme efficiency for metabolism of bufuralol and dextromethorphan by the Trp75Ala mutant compared with CYP2D6*1. In stopped-flow measurements, k_{off} for dextromethorphan was decreased in the absence of Trp75. Our results support a role for Trp75 in substrate shuttling to the active site of CYP2D6.

SIGNIFICANCE STATEMENT

Using combined molecular dynamics and in vitro assays, this study shows for the first time a role for Trp75 as a channel entrance gating residue in the mechanism of substrate binding/unbinding in CYP2D6. Energy landscapes derived from molecular dynamics were used to quantitate the strength of gating, and kinetics assays showed the impact on enzyme efficiency and k_{off} of a Trp75Ala mutation.

Introduction

CYP2D6 is an important member of the drug metabolism class of human cytochromes P450 and is known to metabolize ~15% of currently prescribed pharmaceutical drugs (Guengerich, 2015; Rendic and Guengerich, 2015). Many substrates metabolized by CYP2D6 contain aromatic rings and basic nitrogens, giving them overall positive charge at physiologic pH (Guengerich, 2015). Like most cytochromes P450, CYP2D6 has a buried active site to isolate the active site heme from bulk solvent and to prevent uncoupling reactions (Wade et al., 2004). Understanding substrate and inhibitor access to the CYP2D6 active site is of interest for applications for rational drug design, artificial catalyst design, and better understanding of enzyme structure and function (Dubey et al., 2016; Yu et al., 2016; Fan et al., 2018).

Key insights into CYP2D6 interaction with ligands have come from mutation studies and crystal structures. With 15 crystal structures of CYP2D6 in the Protein Data Bank and a variety of ligands cocrystalized with the enzyme, the conformational flexibility of CYP2D6, as with other cytochromes P450, is becoming more apparent (Rowland *et al.*, 2006; Wang *et al.*, 2012, 2015; https://www.rcsb.org/structure/6CSD). One role of conformational flexibility is to allow substrates to move from the exterior of the enzyme to the active site. Several channels in CYP2D6 have been noted, but they are too small for ligand passage in static measurements (Cojocaru et al., 2007; de Waal et al., 2014; Fischer et al., 2018). However, based on findings in vivo, in vitro, in crystal soaks, and in silico, these channels are known to be pliable to ligands. Further, amino acids that line these channels have been shown to play a role in substrate selectivity, regioselectivity of product formation, and potentially attracting substrates and facilitating substrate movement to the active site (Cojocaru et al., 2007; Johnson and Stout, 2013; Dubey et al., 2016; Yu et al., 2016; Urban et al., 2018; Fischer and Smieško, 2019).

Enzyme flexibility/elasticity allows for high substrate promiscuity as well as access to the active site (Ekroos and Sjogren, 2006; Hritz et al., 2008; Urban et al., 2015; Nair et al., 2016). Amino acids that line the putative egress/access channels, although distal to the active site, are also thought to modulate enzyme activity by affecting which substrates are able to efficiently access the active site (Zhao et al., 2006; Otyepka et al., 2012; Nair et al., 2016; Fischer and Smieško, 2019; Hsu and Johnson, 2019; Li et al., 2020; Xin et al., 2020). Differences in substrate access and product egress routes as observed in molecular dynamics (MD) simulations indicate that cytochromes P450 are adaptable depending on substrate specificities (Lussenburg et al., 2005; Skopalik et al., 2008; de Waal et al., 2014; Hsu and Johnson, 2019; Li et al., 2020; Xin et al., 2020). It is understood that amino acid side chains within substrate

This work was supported by National Institutes of Health National Institute of General Medical Sciences [Grant 2R15GM086767-03] (L.L.F.), a grant to Kalamazoo College from the Sherman Fairchild Foundation, the Heyl Funds of Kalamazoo College, and a grant from the Giving Well Family Foundation.

This work was presented in part at: McCarty KD, Furge KA, and Furge LL (2019) Tryptophan-75 is a potential gating residue of cytochrome P450 2D6. *Great Lakes Drug Metabolism Discussion Group;* 2019 May 9-10; Ann Arbor, MI.

https://doi.org/10.1124/dmd.120.000274.

[S] This article has supplemental material available at dmd.aspetjournals.org.

ABBREVIATIONS: MD, molecular dynamics; P450, cytochrome P450; SNP, single-nucleotide polymorphism.

channels in cytochromes P450 play influential roles in observed drug metabolism and enzyme kinetics (Kingsley and Lill, 2015).

Different roles have been proposed for amino acids that line channels, including tunnel gating and guide rails (Li et al., 2005; Fishelovitch et al., 2009; Zawaira et al., 2011; Shen et al., 2012; Urban et al., 2015; Dubey et al., 2016; Yu et al., 2016; Albertolle et al., 2018; Fan et al., 2018; Fischer and Smieško, 2019). Tunnel gating refers to the flexible amino acid side chain barriers within the active site or substrate channels that control access to the active site, whereas amino acids described as guide rails function via electrostatic interactions to shuttle ligands along channels from the protein's surface to the buried active site. Previous in silico studies with cytochromes P450 have investigated the role of gating residues in impeding ligand movement through channels (Lüdemann et al., 2000a,b; Fishelovitch et al., 2009; Berka et al., 2012; Dubey et al., 2016; Yu et al., 2016; Fan et al., 2018). Most, but not all, of the gating residues identified in other cytochromes P450 (e.g., 3A4, 2E1, 2A6, 2A13, CYP51, and others) have been phenylalanines (Li et al., 2005; Fishelovitch et al., 2009; Zawaira et al., 2011; Shen et al., 2012; Yu et al., 2016; Fan et al., 2018). There have been limited investigations into likely ligand bottlenecks in 2D6 and their roles in metabolism (de Waal et al., 2014; Fischer et al., 2018; Fischer and Smieško, 2019).

We have previously observed differences in backbone flexibility among CYP2D6 variants in MD simulations (de Waal et al., 2014). Collisions between the ligand and amino acids that line the channels can lead to backbone changes, as we (and others) have observed (Winn et al., 2002; Fischer and Smieško, 2019). This has also been observed in comparisons of crystal structure of the same cytochrome P450 with different ligands (Gay et al., 2011; Halpert, 2011; Shah et al., 2012, 2015, 2016; Maekawa et al., 2017; Hsu and Johnson, 2019; Li et al., 2020). Thus, flexibility of the backbone is important for ligand movement through channels.

Varying degrees of backbone distortion have been observed and correlated with aromatic ring flips and side chain rotations [our observations and those of others (Winn et al., 2002; Ekroos and Sjogren, 2006; Shah et al., 2015, 2016; Hsu and Johnson, 2019)]. With CYP2D6, we would expect similar backbone and conformational change distortions that are not observed in the current reference CYP2D6 crystal structures but can be examined by longer-time-scale MD studies as a ligand egresses/accesses the active site. An understanding of how channels change in conformation during ligand egress/access could help in understanding how cytochromes P450 achieve such profound and broad substrate diversity and wide variation in specificity (Winn et al., 2002).

Previous studies from our laboratory showed channel 2b of CYP2D6 to be the most open channel during time evolution studies from molecular dynamics simulations (de Waal et al., 2014). In the present study, we identified Trp75 in channel 2b as a possible gating and guiding residue for ligand egress/access. MD and kinetic findings presented here provide a better understanding of how enzyme plasticity complements channel accessibility for ligands and affects enzyme overall catalytic efficiency.

Materials and Methods

Chemicals

Bufuralol (mixture of enantiomers) and 1′-hydroxyl bufuralol were obtained from Toronto Research Chemical (Toronto, ON, Canada). Both were reconstituted in water for use in assays described. Dextromethorphan and dextrorphan were purchased from Sigma-Aldrich and reconstituted in ethanol. Ultrapure solvents (water, acetonitrile, and methanol) for liquid chromatography were purchased from EMD Chemicals, Inc. (Gibbstown, NJ). Nickel-nitrilotriacetic acid (NTA) agarose was from Qiagen (Germantown, MD). Potassium phosphate, NADPH, 1,2-didodecanoyl-*sn*-glycero-3-phosphocoline phospholipids, acetonitrile, and all other reagents were purchased from Sigma-Aldrich.

Enzymes

The reference *1 plasmid of CYP2D6 with a four-histidine expression tag on the C terminus was a gift from Professor Emily Scott (University of Michigan). The plasmid was previously prepared by Johnson and colleagues by removal of the N-terminal transmembrane helix of CYP2D6 and replacement of the first 33 residues with MAKKTSSKGKL to increase solubility and reduce aggregation (Wang et al., 2012). P450 NADPH rat reductase plasmid [as described by Hanna et al. (1998)] was a gift from Professor F. Guengerich (Vanderbilt University). The Trp75Ala mutant of CYP2D6 was prepared via site-directed mutagenesis of Trp75 to Ala of the *1 construct by GeneScript, and the mutation was confirmed via plasmid sequencing.

The *1 reference and Trp75Ala mutant were expressed in *Escherichia coli* DH5α cells with a pGro7 plasmid for simultaneous expression of the GroEL and GroES chaperone proteins, as described previously (Wang et al., 2012). Briefly, purification involved preparation of the spheroplasts, column chromatography with a nickel-agarose affinity column, and desalting using Pierce Zeba spin columns. The presence and purity of P450 was monitored at various stages of the expression and purification using reduced-CO spectra.

Recombinant P450 NADPH reductase was also expressed in *E. coli* Topp 3 cells, and purification included preparation of spheroplasts, ADP Sepharose affinity column chromatography, and desalting via dialysis, as previously described (Hanna et al., 1998).

Determination of K_s

Ligand binding studies were completed with bufuralol and dextromethorphan with purified recombinant CYP2D6 or mutant CYP2D6 (1 μM) in potassium phosphate buffer (pH 7.4, 100 mM final), as described previously (Nagy et al., 2011). The solution was split evenly between two quartz cuvettes, and the titration was completed using a Cary 300 dual-beam spectrophotometer at room temperature (Agilent Technologies, Santa Clara, CA). Following baseline correction (350–500 nm), bufuralol (1–250 μM) or dextromethorphan (0.05–64 μM) was titrated into the sample cuvette, and equal volumes of water were added to the reference cuvette. Substrate addition volumes were monitored such that the solvent addition never exceeded 5% v/v. The difference between absorbance maxima and minima for each concentration of substrate was plotted against substrate concentration, and the resulting data were analyzed by a nonlinear regression using KaleidaGraph (Synergy Software, Reading, PA). The dissociation constant, K_s, was determined using the following quadratic binding equation: $[CYP2D6{\bullet}S] = 0.5(K_s + E_t + S_t) - [0.25(K_s + E_t + S_t)^2 - E_tS_t]^{1/2}$, where S_t represents substrate concentration, E_t is the total enzyme concentration, and K_s is the spectral dissociation constant for the reaction CYP2D6 + substrate ƒ CYP2D6•substrate.

Determination of K_m and v_{max}

Kinetic studies were completed by reconstituting purified recombinant CYP2D6 (*1 or Trp75Ala mutant) (0.2 μM) with reductase (0.4 μM) and freshly sonicated 1,2-didodecanoyl-*sn*-glycero-3-phosphocoline phospholipids (30 μM) for 10 minutes at room temperature, as described previously (Glass et al., 2018). Reactions contained varying concentrations of the substrates bufuralol (0–600 μM) or dextromethorphan (0–1000 μM) in potassium phosphate buffer (pH 7.4, 100 mM final). Each reaction mixture was incubated for 3 minutes at 30°C prior to initiation with 15 μl NADPH-generating system (5 mM glucose-6-phosphate, 0.5 mM $NADP^+$, and 0.5 U/ml glucose-6-phosphate dehydrogenase) for a final reaction volume of 100 μl. Reactions were quenched with 20 μl acetonitrile, followed by incubation on ice. Reaction times for each substrate were selected within the linear product formation range. Samples were centrifuged (10,000*g*) for 5 minutes, and the supernatant containing substrate and product was analyzed via high-pressure liquid chromatography using a Waters Symmetry C18 Column (100 Å, 5 μm, 3.9 mm × 150 mm) and a Waters 474 fluorescence detector. Isocratic mobile phases were used in the detection of all products. For bufuralol/hydroxybufuralol, the mobile phase was 30% acetonitrile and 70% water with 1 mM perchloric acid, and for detection, excitation and emission wavelengths of 252 and 302 nm were used. For dextromethorphan/dextrorphan, the mobile phase was 20% acetonitrile in water with 0.8% acetic acid and 0.05% triethylamine, and

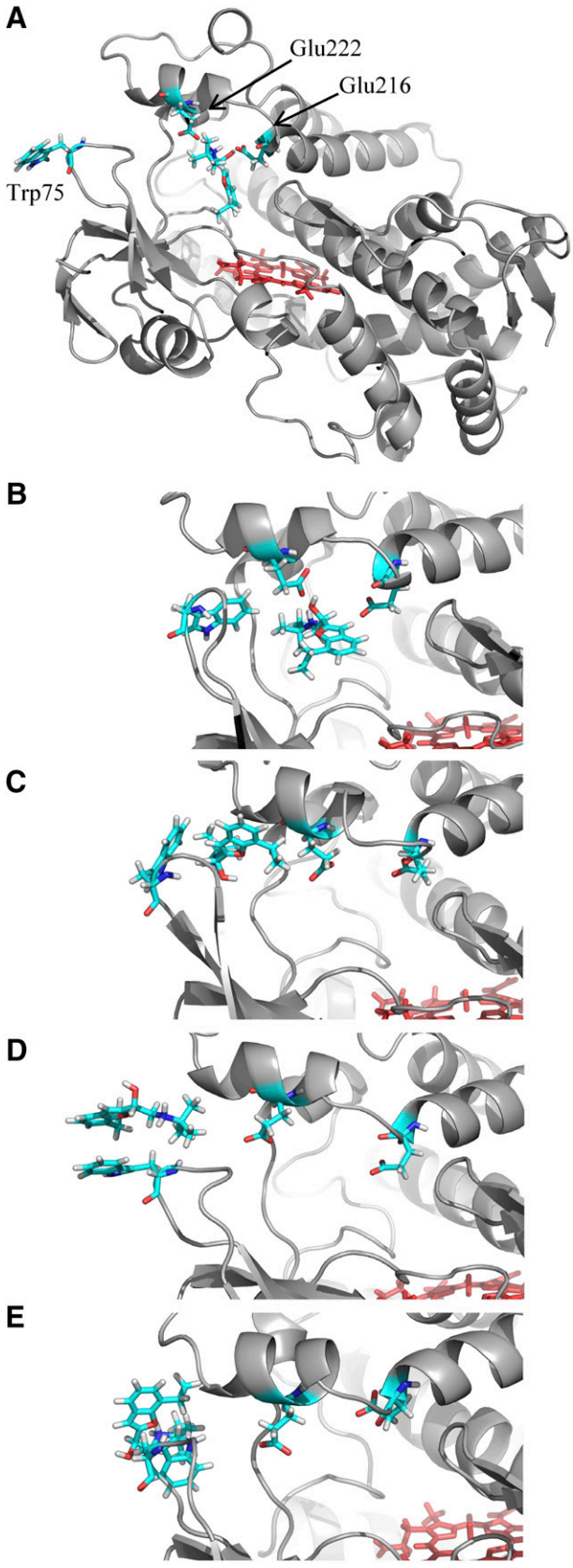

Fig. 1. Bufuralol interacts with Trp75, Glu222, and Glu216 near the opening of channel 2b during egress/access in adaptive biasing simulations. Simulations began with bufuralol docked at the active site. Biasing energy was applied to bufuralol, and movement was restricted to channel 2b. Bufuralol was able to egress from channel 2b and reenter (see Supplemental Fig. 2 for a plot of bufuralol's trajectory and associated simulation frames). All views are of CYP2D6 with bufuralol egressing from the active site shown in slab view. Bufuralol showed the highest contact frequency with Glu216, Glu222, and Trp75 during egress. (A) Bufuralol at ~10 Å from the heme iron. The amino group of bufuralol was 1.6 Å from the carboxylate group of Glu222 and hydrogen bonding. Trp75 was pointed away from the opening of channel 2b. (B) Bufuralol at ~18 Å from the heme iron. The amino group of bufuralol continued to form a hydrogen bond with Glu222 at 1.7 Å, whereas the Trp75 flipped into channel 2b. (C) Bufuralol at ~23 Å from the heme iron and at 3.3 Å from Trp75. The ring edges of Trp75 and bufuralol were perpendicular to each other. (D) As bufuralol exited from channel 2b, face-to-face π-π stacking interactions were formed between the six-member rings of bufuralol and Trp75. (E) After exit of bufuralol from channel 2b, bufuralol reentry could be blocked by Trp75. In this frame, there was π-π stacking between the five-membered rings of bufuralol and Trp75, and Trp75 covered the opening to channel 2b.

for detection, excitation and emission wavelengths of 280 and 310 nm were used. The velocity of product formed per minute per picomole of 2D6 was quantitated using standard curves of 1′-hydroxybufuralol or dextrorphan.

Measurement of k_{off} for Dextromethorphan from CYP2D6*1 or the Trp75Ala Mutant

To measure k_{off} rates for CYP2D6*1 versus the Trp75Ala mutant, stopped-flow spectroscopy was used with purified enzymes and dextromethorphan as model substrate. Dextromethorphan was used in these experiments rather than bufuralol because dextromethorphan showed tighter binding to CYP2D6 than bufuralol in spectral binding titrations. 3-Methoxyphenethylamine was used to displace dextromethorphan upon rapid mixing because it formed a type II binding spectrum with CYP2D6 (Miller et al., 2001) and because the changes from type I (while dextromethorphan was bound) to type II (binding of 3-methoxyphenethylamine) could be monitored over time.

Stopped-flow spectroscopy was completed using a rapid-scanning spectrophotometer OLIS RSM-1000 stopped-flow instrument (On-Line Instrument Systems) in the laboratory of Dr. F. P. Guengerich (Vanderbilt University). Four different reaction conditions were examined: CYP2D6*1 with and without (for control) dextromethorphan and the Trp75Ala mutant with and without (for control) dextromethorphan. One stopped-flow sample syringe contained 4 μM purified CYP2D6*1 or the Trp75Ala mutant with or without 8 μM dextromethorphan and the other 3-methoxyphenethylamine (2000 μM), all in 100 mM potassium phosphate buffer (pH 7.4). Equal volumes from both syringes were injected in the sample cell (4 × 20 mm) at room temperature with a final volume of 2 ml. Absorbance spectra from 350 to 500 nm were recorded at 1-millisecond intervals for a total of 4 seconds. Data were not collected during the initial 4-millisecond mix time. 3-Methoxyphenethylamie produced a type II spectrum upon displacement of dextromethorphan from CYP2D6, and formation of the type II spectrum was used for determining k_{off} for dextromethorphan. To determine k_{off}, data subsets at the absorbance maxima and minima (435 and 410 nm, respectively) were created on the Olis Spectral Works software and then subtracted to create the composite absorbance changes over time ($\Delta A_{410–435}$). Replicates (four to seven for each condition) were averaged and plotted over time to calculate the k_{off} for dextromethorphan.

MD Studies

Model Preparation. The starting structure for CYP2D6 used in MD studies was prepared from 2.8-Å X-ray structure of CYP2D6 bound to prinomastat (PDB ID: 3QM4) (Wang et al., 2012). As previously described, only chain A and its corresponding heme cofactor were used in preparing the *1 reference protein, and crystallographic waters and prinomastat were removed (de Waal et al., 2014). A mutant of CYP2D6 was prepared using the site-directed mutagenesis program Chimera to mutate Trp75 to Ala (http://www.cgl.ucsf.edu/chimera/). For both structures, CYP2D6*1 and the Trp75Ala mutant, bufuralol was used as substrate and was docked using Autodock VINA into the active site cavity of CYP2D6 just above the heme iron.

Biased MD studies were executed using methods previously described (Dickson et al., 2016; de Waal et al., 2020). Briefly, two collective variables, each consisting of four atoms on the molecule or amino acid residue of interest, were selected and designated for biasing. The collective variables were the site of

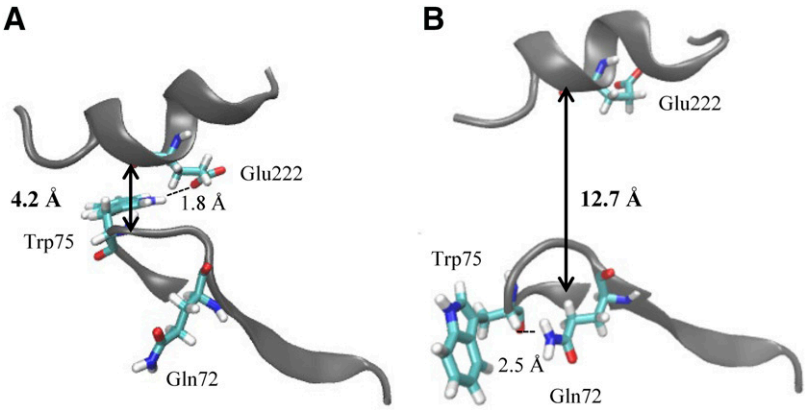

Fig. 2. Impact of hydrogen bonding on channel 2b opening. (A) Hydrogen bonding between Trp75 and Glu222 brought together the loop of the β-1 sheet and helix F′, effectively closing channel 2b. The distance between the backbone atoms was ~4.2 Å. (B) Hydrogen bonding between Trp75 backbone carbonyl and Gln72 resulted in an opening of channel 2b, with the distance between helix F′ and β-1 sheet loop at ~12.7 Å.

molecular biasing during the simulation and were assigned with consideration of several factors. With the substrate bufuralol, the first collective variable was designated as three atoms on the conjugated plate along with a rotatable aliphatic group, and the second was designated along a five-membered chain and consisted of two terminal methyl groups, along with nitrogen and carbon members of the chain (Supplemental Fig. 1A). Atoms of chiral centers were selected over rigid ring structures in bufuralol because biasing around a rotatable bond would cause the ligand to fold and spin rather than exit the protein. For the Trp75 residue, the first collective variable was assigned to four carbon atoms of the six-membered plate of the indole ring, and the second was specified as three carbon atoms and one nitrogen atom of the five-membered plate (Supplemental Fig. 1B). Each of the collective variables were calculated as the root-mean-square deviation between their four constituent atoms and the coordinates of a reference point set near the heme, as in Dickson et al. (2016).

Simulation Protocol. Simulation setup and initiation were performed according to a protocol previously described (de Waal et al., 2014). Setup included equilibration, pressurization, and energy minimization of the model, followed by the designation of the collective variables and parameters, including the biasing parameter b and the radii of cylindrical and spherical restrains, followed by the validation of the model and initiation of the study.

Simulations with Biasing of Bufuralol. Initial MD studies were completed with bufuralol as ligand and with the 2b channel of CYP2D6 restrained as the only pathway of ligand passage (Supplemental Fig. 1C). Channel 2b was selected for these studies because it was the most consistently open channel in time evolution studies previously completed in our laboratory with CYP2D6 variants (de Waal et al., 2014). We previously noted that the F-G loop at the end of channel 2b had a high degree of flexibility (de Waal et al., 2014); the channel also includes parts of substrate recognition site 1 and 2 of CYP2D6, is located directly above the active site in the F-G cassette region (Yu et al., 2013), is near the antechamber identified in crystallography, and has been hypothesized to have a wider range of side chain conformations to adapt to ligand binding (Wang et al., 2015). Simulations began with bufuralol docked in the active site cavity of CYP2D6 (*1 or the Trp75Ala mutant). Adaptive biasing was employed to elicit substrate movement away from the active site cavity. Biasing force was delivered (over a range of biasing parameters, b = 0.85–0.92) to the collective variables of the substrate according to a logarithmic curve throughout the course of the study.

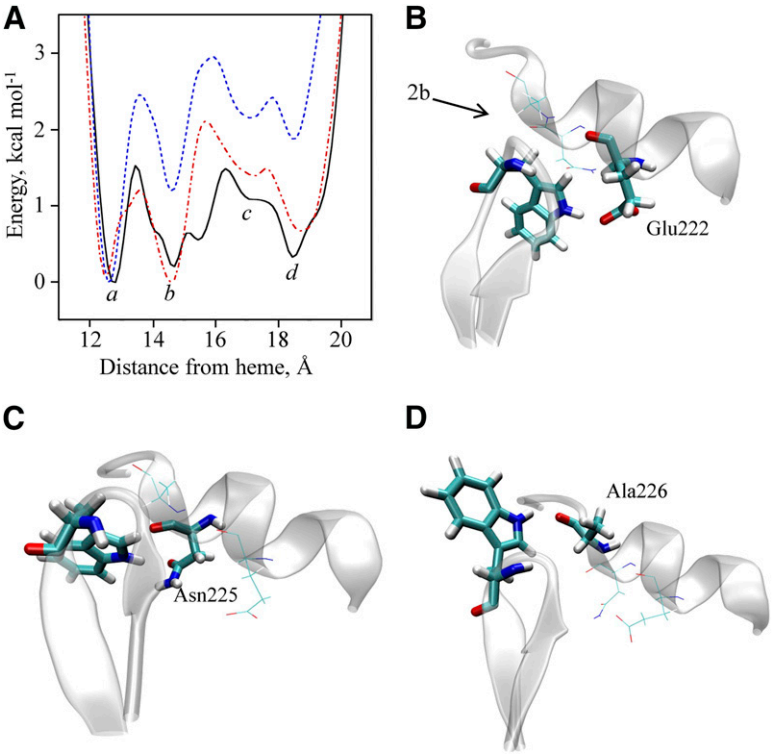

Fig. 3. Reaction coordinate for Trp75 movement and associated conformations. (A) Energy (kilocalories per mole) was tracked for both the first and second collective variable of Trp75 (see Supplemental Fig. 1A) over the course of the reaction coordinate in three separate simulations. The *x*-axis is the distance from the heme center of the collective variables of Trp75. The solid black line represents the lowest biasing energy, and the blue dotted line represents the highest applied biasing energy; the red dotted line is at intermediate biasing energy. The presence of multiple energy wells (four labeled *a*, *b*, *c*, and *d*) suggested multiple stabilized, low-energy-state conformations for Trp75. (B) Representative frame of the lowest energy state, *a*, at 12.8 Å from the heme. At this position, hydrogen bonding between Trp75 and Glu222 blocked ligand passage in channel 2b (entrance to channel 2b toward heme is indicated by arrow). (C) Representative frame of the well at 14.7 Å from the heme, labeled *b* in (A). Trp75 hydrogen-bonded with Asn225 and channel 2b was blocked. (D) Representative frame of the well at 17.3 Å from the heme, labeled *c* in (A). Trp75 hydrogen-bonded with Ala226 and was shifted away from the opening of channel 2b. Multiple fully extended conformations for Trp75, stabilized by hydrophobic interactions, were observed for the low-energy well at 18.5 Å, *d* (frames not shown).

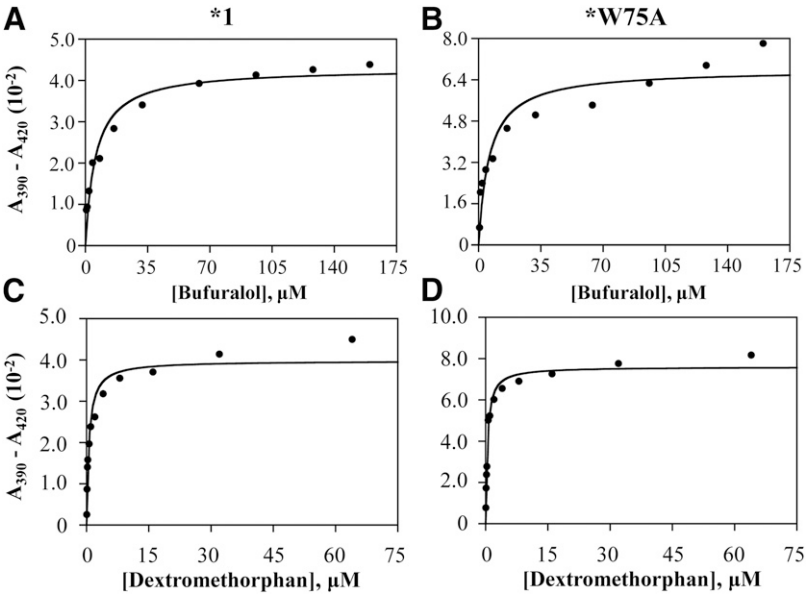

Fig. 4. Determination of spectral binding constants, K_s, for bufuralol and dextromethorphan binding to CYP2D6*1 and a W75A mutant of CYP2D6*1. Both substrates displayed Type 1 binding spectra with each enzyme (data not shown). (A) K_s for bufuralol binding to CYP2D6*1 was 5.7 ± 1.1 μM. (B) K_s for bufuralol binding to the W75A mutant of CYP2D6*1 was 6.0 ± 1.8 μM. (C) K_s for dextromethorphan binding to CYP2D6*1 was 0.60 ± 0.10 μM. (D) K_s for dextromethorpahn binding to the W75A mutant of CYP2D6*1 was 0.40 ± 0.05 μM.

A range of biasing energy settings were tested to determine suitable boundaries for a substrate biasing energy that would allow for sampling of a range of conformations over the course of the 1-microsecond simulation without resulting in substrate stalling in a single conformation/position (too low of biasing energy) or deforming the protein (too high of biasing energy). Additionally, biasing force was capped by an overfill script to prevent the system from delivering more than ~18 kcal/mol of energy to the substrate.

During MD studies, the P450 heme was labeled as a reference point, and the displacement of bufuralol relative to the reference point was tracked as a function of frame number. This information was graphed to identify barriers to substrate movement during the simulation (Supplemental Fig. 2). Graphically, clusters of points and maxima/minima identified potential barriers to bufuralol movement within the protein. When bufuralol encountered a barrier, it either remained at that position or receded back to a previous position, forming local maxima/minima. Clusters of points, where the displacement value did not change as simulation time passed, were formed when bufuralol movement was restricted and typically resulted from molecular interactions between bufuralol and the enzyme. Simulation mapping was employed 1) to determine the location of barriers (given by displacement values) to bufuralol movement and 2) to identify frame numbers in which bufuralol movement along the 2b channel was halted. In addition, the simulation was analyzed to determine which residues bufuralol contacted most frequently. The Visual Molecular Dynamics software tool contactFreq.tcl (https://www.ks.uiuc.edu/Research/vmd/mailing_list/vmd-l/19311.html) was used to analyze the trajectory of the bufuralol and determine the amino acids that the substrate contacted. Contact frequency was reported as the relative frequency of interactions between bufuralol and individual residues. Residues with high contact frequencies were considered as possible energy barriers to substrate movement. Frames in which bufuralol was interacting with these residues were selected and further analyzed with Binding Analyzer (BINANA) (Durrant and McCammon, 2011). BINANA was used to identify intermolecular interactions between bufuralol and enzyme amino acid residues in a given frame of the simulation. From these data, we were able to determine which amino acid residues interacted with bufuralol during substrate movement within the 2b channel of CYP2D6.

Simulations with bufuralol and CYP2D6*1 were completed first, and the same biasing parameters used in simulations with *1 were then used in simulations with bufuralol and the Trp75Ala mutant. To test whether the absence of Trp75 allowed for different (lower) biasing potentials to be applied, we also completed three simulations at lower biasing potentials with bufuralol and the Trp75Ala mutant. At lower biasing potentials, bufuralol did not egress; thus, we used the same biasing potentials with the Trp75Ala mutant as we used with *1.

Simulations with Biasing of Trp75. To analyze the movements and conformations of Trp75 that may contribute to substrate movement along channel 2b, MD studies with biasing energy applied to Trp75 were completed. All simulations were started with the Trp75 facing inward to channel 2b and the F′ helix (Supplemental Fig. 3). In one set of simulations (greater than nine replicates), the F′ helix was unrestrained, allowing full fluctuation in size and conformation of the channel 2b opening/closing between the F′ helix and β-1 sheet. In addition, to capture consistent energy landscapes for calculating energy associated with Trp75 conformational changes over the course of a simulation, in some simulations (greater than five replicates), the F′ helix was restrained in a conformation consistent with a more closed channel 2b. Energy landscapes of Trp75 were determined by calculating the potential of mean force along the second collective variable from the free energies computed by the simulations. Energy wells in the graph were identified as stable states of Trp75 and were used in conjunction with simulation mapping, contact frequency analysis, and BINANA to identify the stable conformations of Trp75.

Criteria for conformational changes were based on measured changes in the distance moved by the collective atoms of Trp75 relative to a fixed point, usually the heme iron. For comparing the conformational flexibility of each individual tryptophan in CYP2D6, movement was measured relative to the initial position of each tryptophan in the simulation with no biasing energy applied.

Molecular Visualization

PyMOL 3.1.0 and Visual Molecular Dynamics software were used in enzyme visualization and for figure preparation.

TABLE 1

Summary of spectral binding and kinetic parameters for bufuralol binding and metabolism, respectively, by CYP2D6 enzymes

Parameter	2D6*1	Trp75Ala Mutant
K_s (μM)	5.7 ± 1.1	6.0 ± 1.8
v_{max} (min^{-1})	2.3 ± 0.1	3.0 ± 0.1
K_m (μM)	33 ± 7	89 ± 8
Efficiency[a]	0.07	0.03

[a]Efficiency defined as v_{max}/K_m with units of $minute^{-1}$ $micromolar^{-1}$.

Results

Bufuralol Movement along Channel 2b in CYP2D6*1 in MD Simulations. Initial biased MD studies of CYP2D6*1 were performed with bufuralol as substrate and with the 2b channel restrained as the only pathway of substrate passage [channel nomenclature of Wade (Cojocaru et al., 2007)]. Bufuralol, a prescription β-blocker, was selected for our studies because it contains the characteristics of most CYP2D6

substrates: aromatic rings, a basic nitrogen, several degrees of bond rotation available, and a typical molecular weight (261 g/mol). Bufuralol is also one of the most widely used substrates in the characterization of CYP2D6 activity in the literature.

In MD simulations, bufuralol fully egressed from 2D6*1 and was also able to reenter the channel and move toward the active site. Resulting simulations were reviewed for their contact frequency to understand barriers to substrate movement.

Three residues were key effectors of bufuralol movement within channel 2b: Glu216, Glu222, and Trp75. The acidic residues Glu216 and Glu222 both reside on the F helix in the interior of the enzyme, whereas the hydrophobic Trp75 is on the loop connecting the β-sheets β1-1 and β1-2 near the surface of the enzyme (in vivo, this would be positioned in the lipid membrane). When bufuralol was unable to egress from CYP2D6*1, it made the largest frequency of contact with Glu216 and Glu222 (Fig. 1). When bufuralol did egress, the substrate made contact most frequently with Trp75 (Fig. 1). Further analysis via the BINANA script showed that hydrogen-bonding events between the acidic glutamic acid residues and the basic nitrogen atom of bufuralol created binding events that controlled substrate movement within 2b. In all simulations, interactions between Trp75 and bufuralol consisted of multiple types of interactions, including hydrogen bonding with backbone and R groups and cation-π and π-π interactions (Fig. 1). Bufuralol reentry into channel 2b followed essentially reversed amino acid contacts.

Bufuralol Movement along Channel 2b in a Trp75Ala Mutant of CYP2D6*1 in MD Simulations. MD simulations with biasing of bufuralol were conducted with a Trp75Ala mutant of CYP2D6*1 in the same manner as with *1. The alanine substitution at residue 75 did not alter the level of biasing required for bufuralol to egress from the mutant CYP2D6, and the same biasing potentials were used, as indicated in the *Materials and Methods*. Analysis of the contact frequency showed that in the absence of Trp75, Glu216 was the most frequently contacted residue by bufuralol. Further analysis with the BINANA script confirmed that hydrogen-bonding events between residues Glu216 and Glu222 with bufuralol were responsible for energy barriers to substrate movement within channel 2b of the Trp75Ala CYP2D6 mutant (data not shown).

Analysis of Trp75 Conformations in MD Simulations with CYP2D6*1. Given the contact frequency between bufuralol and Trp75, as well as the multiple conformations adopted by Trp75 during simulations, MD studies with biasing of Trp75 were completed. As mentioned in the *Materials and Methods*, in one set of simulations, the F′ helix was allowed unrestrained movement to reveal the breadth of conformations available. Then, to quantitate energy changes associated more specifically with Trp75 conformational changes, the F′ helix was restrained in additional simulations. In both sets of simulations, molecular visualization revealed that Trp75 transitioned frequently between various conformations and that it had a wide range of movement in three-dimensional space. For comparison, we also examined movement and position of the other five CYP2D6 tryptophan residues in simulations (at positions 128, 152, 262, 316, and 409). In all cases, these other tryptophans showed little to no conformational flexibility or movement (typically moving no more than the length of a hydrogen bond) compared with Trp75, which displayed a range of motion of up to 20 Å (Supplemental Fig. 4).

In molecular visualization from simulations in which the F′ helix was not restrained, hydrogen bonding between the indole ring of Trp75 (hydrogen bond donor) and the carbonyl side chain of Glu222 (hydrogen bond acceptor) was observed and projected Trp75 into channel 2b (Fig. 2A). By contact frequency analysis, this was the most common interaction for Trp75 when the F′ helix was unrestrained. Hydrogen bond interactions between the backbone amino group of Trp75 and the carbonyl of the R-group of Gln72 stabilized an open channel 2b (Fig. 2B). To hydrogen-bond with Gln72, the amino group of Trp75 had to be less than 2.5 Å away from the carbonyl acceptor of Gln72. Thus, a large degree of backbone flexibility was required. Most conformations of Trp75 were not able to form the interaction with Gln72 because the distance from the donor to the acceptor was typically >8 Å.

Further analysis showed that the F′ helix can bend downward into channel 2b, or pitch upward away from the channel, and that Trp75 movement largely coincided with movement of the F′ helix when it was unrestrained. Transition of channel 2b from closed to open conformations nearly tripled the distance between the F′ helix backbone and the backbone of the β1-1/β1-2 loop with Trp75 (Fig. 2). The increased opening of the channel was then observed to facilitate substrate entrance and exit from CYP2D6 in simulations.

From simulations in which the F′ helix was restrained, it was possible to generate an energy landscape for Trp75. The energy landscapes produced suggested that Trp75 adopted four low-energy stable conformations located at approximately 12.8-, 14.7-, 17.3-, and 18.5-Å displacements from the heme to the collective variables of Trp75 (Fig. 4A; Supplemental Fig. 1B). The overall free-energy change for Trp75 conformations was −3 kcal/mol, correlating with the energy of a typical hydrogen bond. The average free-energy change between the lowest-energy Trp75 conformations was around −1 kcal/mol (Fig. 3A). Representative frames for conformations at the bottom of each energy well showed different stabilizing interactions (Fig. 3). At 12.8 Å, Trp75 hydrogen-bonded with the carboxylate group of Glu222 and blocks channel 2b (Fig. 3B). At 14.7 Å, Trp75 hydrogen-bonded with the guanidino group of Asn225 and also blocked channel 2b (Fig. 3C). At 17.3 Å, Trp75 hydrogen-bonded with the backbone carbonyl of Ala226 but was shifted away from the opening of channel 2b (Fig. 3D). At 18.5 Å, Trp75 was the most extended from the protein core and sampled multiple conformations and hydrophobic interactions with multiple residues including those at the (modified for crystallography) N-terminal end of the enzyme (what would be Pro41 and Gly42 of full-length sequence). In simulations in which the F′ helix was not restrained,

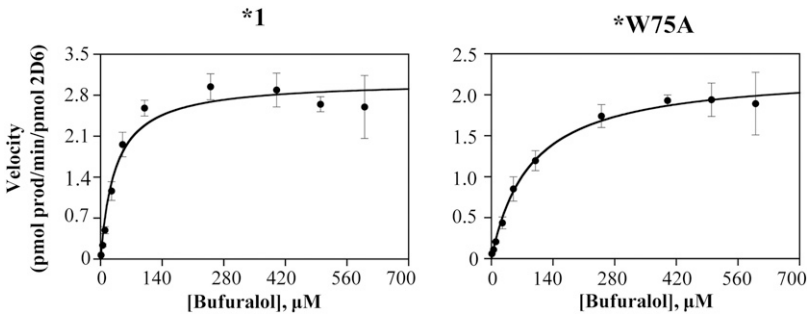

Fig. 5. Michaelis-Menten kinetic analysis. Kinetic studies were completed by reconstituting purified recombinant CYP2D6 (*1 or Trp75Ala mutant) (0.2 μM) with reductase (0.4 μM) and freshly sonicated 1,2-didodecanoyl-*sn*-glycero-3-phosphocoline phospholipids (30 μM) for 10 minutes at room temperature as described previously (Glass et al., 2018). Reactions contained varying concentrations of bufuralol (0–600 μM) as indicated. Each reaction mixture was incubated for 3 minutes at 30°C prior to initiation with the NADPH-generating system. Reactions were quenched with acetonitrile. K_m and v_{max} values for CYP2D6*1 with bufuralol were 33 ± 7 μM and 2.3 ± 0.1 minutes^{-1}, respectively. K_m and v_{max} for the Trp75Ala mutant of CYP2D6*1 with bufuralol were 89 ± 8 μM and 3.0 ± 0.1 minutes^{-1}, respectively. Each point represents the S.D. for experiments completed in quadruplicate.

a hydrogen bond was able to form between the backbone carbonyl of Trp75 and the amide group of Gln72. When Trp75 was in the fully extended position, channel 2b was not blocked. From contact frequency analysis when the F′ helix was restrained, Trp75 most frequently interacted with Ala226, followed by Asn225 and then Glu222.

Expression and Purification of CYP2D6 Enzymes. To better understand the roles of Trp75 in ligand interaction with CYP2D6, CYP2D6*1 and a Trp75Ala mutant of CYP2D6*1 were prepared and studied in reconstituted enzyme systems, as described in the *Materials and Methods*. Expression of CYP2D6 enzymes yielded ~600 nmol/l in whole cells for both *1 and the Trp75Ala mutant, and the final concentration of purified CYP2D6 was 150 and 160 μM for *1 and Trp75Ala, respectively. Little or no spectral peak at 420 nm was observed in purifed samples (data not shown).

Spectral Binding Titrations. Titration of CYP2D6 enzymes (*1 and the Trp75Ala mutant) with the substrates bufuralol and dextromethorphan resulted in type I binding spectra in both cases (data not shown). Plots of the difference between absorbance maxima and minima for each concentration of substrate were fitted to the quadratic velocity equation to yield the K_s values for bufuralol and dextromethorphan with CYP2D6*1 of 5.7 ± 1.1 and 0.60 ± 0.10 μM, respectively (Fig. 4; Table 1). With the Trp75Ala mutant, the K_s values for bufuralol and dextromethorphan were 6.0 ± 1.8 and 0.40 ± 0.05 μM, respectively (Fig. 4; Table 1).

Measurement of k_{off} of Dextromethorphan. Since dextromethorphan was a tighter binding substrate in spectral binding titrations, dextromethorphan was used in stopped-flow spectroscopy to measure the k_{off} from CYP2D6*1 and the Trp75Ala mutant as described in the *Materials and Methods*. For CYP2D6*1, the k_{off} was 28 ± 4 seconds^{-1}, and for the Trp75Ala mutant, the rate was lower, at 14.4 ± 0.6 seconds^{-1} (Supplemental Fig. 5).

Michaelis-Menten Kinetics. CYP2D6 enzymes were analyzed for their Michaelis-Menten kinetic properties with bufuralol. Both CYP2D6 *1 and the Trp75Ala mutant were active in the conversion of bufuralol to 2-hydroxybufuralol and followed traditional Michaelis-Menten hyperbolic curves (Fig. 5). The K_m value for bufuralol with CYP2D6*1 was 33 ± 7 μM. With the Trp75Ala mutant, K_m for bufuralol was 89 ± 8 μM (Table 1). Additionally, the v_{max} value for bufuralol with CYP2D6*1 was determined to be 2.3 ± 0.1 minutes^{-1}. With the Trp75Ala mutant, the v_{max} value was 3.0 ± 0.1 minutes^{-1} (Table 1).

Resulting catalytic efficiency, defined as v_{max}/K_m, for bufuralol with CYP2D6*1 was 0.07 minutes^{-1} μM^{-1}. For the Trp75Ala mutant, v_{max}/K_m for bufuralol was lower, at 0.03 minutes^{-1} μM^{-1} (Table 1). For comparison, dextromethorphan metabolism to dextrorphan was also measured. As with bufuralol, the overall efficiency was lower for the Trp75Ala mutant (0.05 minutes^{-1} μM^{-1} for *1 vs. 0.03 minutes^{-1} μM^{-1} for the mutant; data not shown).

Discussion

There are several different terms used in the literature—gating, gatekeeper, revolving door, clamps, ceiling, guiding rail, etc.—to describe amino acids, usually large aromatic rings like Phe, that must change conformation to accommodate movement of substrates/inhibitors along cytochrome P450 ligand egress/access channels. These low-energy conformations are stabilized most commonly by hydrogen bonds and π-π stacking between ligands and the amino acids with which they interact. Trp75 has previously been noted to line the entrance to channel 2b of CYP2D6 (Wang et al., 2015), but no role in ligand shuttling has been described. The present study determined that Trp75 could facilitate substrate movement and metabolism by CYP2D6. The residue was observed not only to impact the in vitro kinetics of CYP2D6 but also to be involved in egress and access of substrates in the enzyme along channel 2b in MD studies, and mutation of the residue resulted in modest reduction in enzyme efficiency in vitro.

In our MD simulations, Trp75 appeared to work in tandem with Glu222 and Glu216 to facilitate substrate mobility through channel 2b into the active site cavity as part of a guide rail system or substrate shuttle. The substrate shuttle was described by the movement of substrates to the active site cavity through hydrogen bond interactions with a cascade of anionic residues (including Glu222 and Glu216). Glu222 and Glu216 also slowed ligand exit from the same channel, as determined by contact frequency calculations. In simulations with the Trp75Ala mutant, bufuralol made the most contacts with Glu216 and did not egress as effectively as when Trp75 was present. Wang et al. (2012) have previously shown that Glu222 forms part of the polar surface of the F′ helix and is able to change conformation to orient toward the interior (toward the active site) of CYP2D6 or away. Observations that the hydrogen-bonding energy barrier created by these residues to substrate egress was only overcome using larger biasing potentials on bufuralol support this theory. Conversely, when bufuralol did egress from CYP2D6 in simulations, Trp75 was the most contacted residue.

Other research has shown that Glu222 and Glu216, along with Phe120 and Asp301, play a crucial role in substrate transport, substrate orientation into the active site cavity, and the resulting stereochemistry of product (Guengerich et al., 2003; Paine et al., 2003; Flanagan et al., 2004; Masuda et al., 2006). Because the presence of a basic nitrogen group characterizes most substrates of CYP2D6, Glu216, Glu222, and Asp301 appear to be relevant in substrate transport within channel 2b, and in their absence, rates of catalysis are decreased (Guengerich et al., 2002, 2003; Paine et al., 2003). Studies of these amino acids have shown that successive hydrogen bonds down this cascade of anionic residues induce a conformational change in the 2b channel, potentially increasing the energetic favorability for the ligand to enter the active site cavity (Wang et al., 2015). Wang et al. (2015) found that a Glu222Ala mutation resulted in no change in the K_m of the system but decreased the v_{max} and suggested that the mutation disrupted the cascade of anionic residues within the channel that form the proposed shuttle, slowing substrate passage and explaining the decrease in v_{max} observed for the Glu222Ala mutant.

Phe120, unlike the other three residues, is a bulky hydrophobic residue near the active site that is capable of forming π-π stacking interactions with ligands necessary for both orientation of ligands and facilitating movement. In addition, Phe120 decreases the flexibility of the BC loop that is part of channel 2. In the absence of Phe120, as in the naturally occurring CYP2D6*53 variant, the BC loop is more flexible, and rates of catalysis are approximately one order of magnitude greater (de Waal et al., 2014; Don and Smieško, 2018; Glass et al., 2018). Also, substrate metabolites formed by the *53 variant vary from those found by CYP2D6*1 (Flanagan et al., 2004; Glass et al., 2018).

Building off these findings, we propose that Trp75 interacts with substrates at the entry point to channel 2b and aids in initial shuttling of substrates into the active site as well as the reverse steps of egress via a "push and pull" of ligands at the mouth of channel 2b. Our proposed mechanism is based on the observed interactions between bufuralol and Trp75 and other amino acids in MD simulations and on kinetic findings with a Trp75Ala mutant of CYP2D6. The observed MD interactions were as follows: 1) Trp75 adopted a conformation that was stabilized by interactions with Gln72, Ala226, or hydrophobic interactions on the β-1 sheet and that left channel 2b open (Figs. 2 and 3); 2) Trp75 encountered a substrate and interacted via hydrogen bond donating of the indole ring and π-π stacking of aromatic rings (Fig. 1); 3) substrate binding disrupted the Trp75 hydrogen bond with Gln72, destabilizing that Trp75

conformation; 4) Trp75 transitioned to a conformation that capped the end of channel 2b; 5) Trp75 was stabilized by interactions with amino acids on the F′ helix, and the substrate was shuttled from Trp75 to the active site cavity through hydrogen bond interactions with anionic residues Glu222, Glu216, and Asp301 and oriented for metabolism by interactions with Phe120 as well. Trp75 (by initially interacting with substrate, as in Fig. 1E) and Glu222 and Glu216 (by hydrogen bonding and pulling the substrate into active site cavity, as in Fig. 1, A and B) worked in tandem to facilitate substrate entrance into channel 2b, albeit with low-energy interactions (hydrogen bond and π-π stacking) (Fig. 3).

The change in k_{off} and enzymatic efficiency between *1 and the Trp75Ala mutant supports this idea. In the absence of Trp75, substrate departure would be slowed (e.g., not as readily pulled out of active site and slower k_{off} as observed), and substrates would spend more time in the active site and, as a result, lead to greater enzymatic efficiency with CYP2D6 with Trp75 present (*1) than without it (the Trp75Ala mutant) (Table 1). Measurement of k_{off} rates with CYP2D6*1 and the Trp75Ala mutant show that k_{off} is decreased by half in the absence of Trp75. This finding supports the hypothesis that Trp75 can aid in pushing and pulling ligands at the channel of 2b, although we are cautious not to overinterpret the results, because the effect was modest. Also, in the absence of Trp75, the stabilizing interactions between the loop of β-chains (via Trp75) and the F′ helix across channel 2b (via residues Glu222, Ala226, and Asn225) were not formed, leading to the observation of a wider channel 2b opening (Fig. 2), consistent with altered flexibility of this region of the enzyme and impacting ligand flux.

This model is similar to those reported from MD studies with human CYP51 and bacterial BM3; in those studies, ligands were only able to move out of the substrate channel in coordination with flexible movement of residues at the entrance to the channel (Dubey et al., 2016; Yu et al., 2016). Furthermore, the noted flexible movement of the residues at the entrance to the channels was postulated to have a role in keeping the substrate in the active site for catalysis. From clinical observations, patients with a single-nucleotide polymorphism (SNP) in CYP2D6 near the opening of channel 2b (on the F-G loop) show reduced efficacy in antidepressant metabolism, for instance (Xin et al., 2020). Xin et al. (2020) suggest the reduced efficacy is due to decreased ability of substrates to enter the substrate access channel at that position. It is expected that other SNPs along the channels of CYP2D6 could impact substrate metabolism, with the most well understood channel SNP being Phe120Ile, which is in the CYP2D6*53 variant and leads to an ultrametabolizer phenotype (de Waal et al., 2014; Glass et al., 2018). Other than CYP2D6*53, the most common CYP2D6 amino acid variants do not appear to line channels but could impact metabolism by distal effects on enzyme flexibility/plasticity and consequently enzyme stability.

In vivo, Trp75 would be expected to be buried in the lipid membrane, the putative access point for hydrophobic substrates. The 15 crystal structures of CYP2D6 show wide variation of dihedral angles for Trp75—even within the same structure but different chains (example in Supplemental Fig. 6). Our data, in combination with crystallography that has shown a second ligand binding site in the antechamber region of CYP2D6 (e.g., same area as channel 2b), also suggest that the gating of a substrate channel by Trp75 may keep ligands moving toward the active site for catalysis. Kinetic data also support that finding because the enzyme efficiency decreases in the Trp75Ala mutant.

Urban et al. (2018) reviewed studies on ligand access channels in P450s and concluded that aromatic residues in particular may serve an important role in ligand access to channels. Our findings support that conclusion and identify Trp75 of CYP2D6 as an aromatic residue involved in substrate recognition and shuttling. Our studies further use in vitro approaches to "bridge the gap" to in silico studies.

Acknowledgments

We thank Dr. Parker de Waal (David E. Shaw Research) and Dr. Brad Dickson (Van Andel Research Institute) for helpful discussions involving the implementation and interpretation of the molecular dynamics experiments and Dr. Fred Guengerich (Vanderbilt University) for help with stopped-flow experiments.

Authorship Contributions

Participated in research design: McCarty, Ratliff, K. A. Furge, L. L. Furge.
Conducted experiments: McCarty, Ratliff, K. A. Furge.
Performed data analysis: McCarty, Ratliff, K. A. Furge, L. L. Furge.
Wrote or contributed to the writing of the manuscript: McCarty, Ratliff, K. A. Furge, L. L. Furge.

References

Albertolle ME, Phan TTN, Pozzi A, and Guengerich FP (2018) Sulfenylation of human liver and kidney microsomal cytochromes P450 and other drug-metabolizing enzymes as a response to redox alteration. *Mol Cell Proteomics* **17**:889–900.
Berka K, Hanák O, Sehnal D, Banás P, Navrátilová V, Jaiswal D, Ionescu CM, Svobodová Vareková R, Koca J, and Otyepka M (2012) MOLEonline 2.0: interactive web-based analysis of biomacromolecular channels. *Nucleic Acids Res* **40**:W222–W227.
Cojocaru V, Winn PJ, and Wade RC (2007) The ins and outs of cytochrome P450s. *Biochim Biophys Acta* **1770**:390–401.
de Waal PW, Shi J, You E, Wang X, Melcher K, Jiang Y, Xu HE, and Dickson BM (2020) Molecular mechanisms of fentanyl mediated β-arrestin biased signaling. *PLOS Comput Biol* **16**: e1007394.
de Waal PW, Sunden KF, and Furge LL (2014) Molecular dynamics of CYP2D6 polymorphisms in the absence and presence of a mechanism-based inactivator reveals changes in local flexibility and dominant substrate access channels. *PLoS One* **9**:e108607.
Dickson BM, de Waal PW, Ramjan ZH, Xu HE, and Rothbart SB (2016) A fast, open source implementation of adaptive biasing potentials uncovers a ligand design strategy for the chromatin regulator BRD4. *J Chem Phys* **145**:154113.
Don CG and Smieško M (2018) Microsecond MD simulations of human CYP2D6 wild-type and five allelic variants reveal mechanistic insights on the function. *PLoS One* **13**:e0202534.
Dubey KD, Wang B, and Shaik S (2016) Molecular dynamics and QM/MM calculations predict the substrate-induced gating of cytochrome P450 BM3 and the regio- and stereoselectivity of fatty acid hydroxylation. *J Am Chem Soc* **138**:837–845.
Durrant JD and McCammon JA (2011) BINANA: a novel algorithm for ligand-binding characterization. *J Mol Graph Model* **29**:888–893.
Ekroos M and Sjögren T (2006) Structural basis for ligand promiscuity in cytochrome P450 3A4. *Proc Natl Acad Sci USA* **103**:13682–13687.
Fan JR, Li H, Zhang HX, and Zheng QC (2018) Exploring the structure characteristics and major channels of cytochrome P450 2A6, 2A13, and 2E1 with pilocarpine. *Biopolymers* **109**:e23108.
Fischer A, Don CG, and Smieško M (2018) Molecular dynamics simulations reveal structural differences among allelic variants of membrane-anchored cytochrome P450 2D6. *J Chem Inf Model* **58**:1962–1975.
Fischer A and Smieško M (2019) Spontaneous ligand access events to membrane-bound cytochrome P450 2D6 sampled at atomic resolution. *Sci Rep* **9**:16411.
Fishelovitch D, Shaik S, Wolfson HJ, and Nussinov R (2009) Theoretical characterization of substrate access/exit channels in the human cytochrome P450 3A4 enzyme: involvement of phenylalanine residues in the gating mechanism. *J Phys Chem B* **113**:13018–13025.
Flanagan JU, Maréchal JD, Ward R, Kemp CA, McLaughlin LA, Sutcliffe MJ, Roberts GC, Paine MJ, and Wolf CR (2004) Phe120 contributes to the regiospecificity of cytochrome P450 2D6: mutation leads to the formation of a novel dextromethorphan metabolite. *Biochem J* **380**:353–360.
Gay SC, Zhang H, Wilderman PR, Roberts AG, Liu T, Li S, Lin HL, Zhang Q, Woods VL Jr, Stout CD, et al. (2011) Structural analysis of mammalian cytochrome P450 2B4 covalently bound to the mechanism-based inactivator tert-butylphenylacetylene: insight into partial enzymatic activity. *Biochemistry* **50**:4903–4911.
Glass SM, Martell CM, Oswalt AK, Osorio-Vasquez V, Cho C, Hicks MJ, Mills JM, Fujiwara R, Glista MJ, Kamath SS, et al. (2018) CYP2D6 allelic variants *34, *17-2, *17-3, and *53 and a Thr309Ala mutant display altered kinetics and NADPH coupling in metabolism of bufuralol and dextromethorphan and altered susceptibility to inactivation by SCH 66712. *Drug Metab Dispos* **46**:1106–1117.
Guengerich FP (2015) Human cytochrome P450 enzymes, in *Cytochrome P450: Structure, Mechanism, and Biochemistry* (Ortiz de Montellano PR ed), pp 523–786, Springer, New York.
Guengerich FP, Hanna IH, Martin MV, and Gillam EM (2003) Role of glutamic acid 216 in cytochrome P450 2D6 substrate binding and catalysis. *Biochemistry* **42**:1245–1253.
Guengerich FP, Miller GP, Hanna IH, Martin MV, Léger S, Black C, Chauret N, Silva JM, Trimble LA, Yergey JA, et al. (2002) Diversity in the oxidation of substrates by cytochrome P450 2D6: lack of an obligatory role of aspartate 301-substrate electrostatic bonding. *Biochemistry* **41**:11025–11034.
Halpert JR (2011) Structure and function of cytochromes P450 2B: from mechanism-based inactivators to X-ray crystal structures and back. *Drug Metab Dispos* **39**:1113–1121.
Hanna IH, Teiber JF, Kokones KL, and Hollenberg PF (1998) Role of the alanine at position 363 of cytochrome P450 2B2 in influencing the NADPH- and hydroperoxide-supported activities. *Arch Biochem Biophys* **350**:324–332.
Hritz J, de Ruiter A, and Oostenbrink C (2008) Impact of plasticity and flexibility on docking results for cytochrome P450 2D6: a combined approach of molecular dynamics and ligand docking. *J Med Chem* **51**:7469–7477.
Hsu MH and Johnson EF (2019) Active-site differences between substrate-free and ritonavir-bound cytochrome P450 (CYP) 3A5 reveal plasticity differences between CYP3A5 and CYP3A4. *J Biol Chem* **294**:8015–8022.
Johnson EF and Stout CD (2013) Structural diversity of eukaryotic membrane cytochrome p450s. *J Biol Chem* **288**:17082–17090.
Kingsley LJ and Lill MA (2015) Substrate tunnels in enzymes: structure-function relationships and computational methodology. *Proteins* **83**:599–611.

Li J, Zhou Y, Tang Y, Li W, and Tu Y (2020) Dissecting the structural plasticity and dynamics of cytochrome P450 2B4 by molecular dynamics simulations. *J Chem Inf Model* **60**:5026–5035 DOI: 10.1021/acs.jcim.0c00482.

Li W, Liu H, Scott EE, Gräter F, Halpert JR, Luo X, Shen J, and Jiang H (2005) Possible pathway(s) of testosterone egress from the active site of cytochrome P450 2B1: a steered molecular dynamics simulation. *Drug Metab Dispos* **33**:910–919.

Lüdemann SK, Lounnas V, and Wade RC (2000a) How do substrates enter and products exit the buried active site of cytochrome P450cam? 1. Random expulsion molecular dynamics investigation of ligand access channels and mechanisms. *J Mol Biol* **303**:797–811.

Lüdemann SK, Lounnas V, and Wade RC (2000b) How do substrates enter and products exit the buried active site of cytochrome P450cam? 2. Steered molecular dynamics and adiabatic mapping of substrate pathways. *J Mol Biol* **303**:813–830.

Lussenburg BM, Keizers PH, de Graaf C, Hidestrand M, Ingelman-Sundberg M, Vermeulen NP, and Commandeur JN (2005) The role of phenylalanine 483 in cytochrome P450 2D6 is strongly substrate dependent. *Biochem Pharmacol* **70**:1253–1261.

Maekawa K, Adachi M, Matsuzawa Y, Zhang Q, Kuroki R, Saito Y, and Shah MB (2017) Structural basis of single-nucleotide polymorphisms in cytochrome P450 2C9. *Biochemistry* **56**: 5476–5480.

Masuda K, Tamagake K, Katsu T, Torigoe F, Saito K, Hanioka N, Yamano S, Yamamoto S, and Narimatsu S (2006) Roles of phenylalanine at position 120 and glutamic acid at position 222 in the oxidation of chiral substrates by cytochrome P450 2D6. *Chirality* **18**:167–176.

Miller GP, Hanna IH, Nishimura Y, and Guengerich FP (2001) Oxidation of phenethylamine derivatives by cytochrome P450 2D6: the issue of substrate protonation in binding and catalysis. *Biochemistry* **40**:14215–14223.

Nagy LD, Mocny CS, Diffenderfer LE, Hsi DJ, Butler BF, Arthur EJ, Fletke KJ, Palamanda JR, Nomeir AA, and Furge LL (2011) Substituted imidazole of 5-fluoro-2-[4-[(2-phenyl-1H-imidazol-5-yl)methyl]-1-piperazinyl]pyrimidine Inactivates cytochrome P450 2D6 by protein adduction. *Drug Metab Dispos* **39**:974–983.

Nair PC, McKinnon RA, and Miners JO (2016) Cytochrome P450 structure-function: insights from molecular dynamics simulations. *Drug Metab Rev* **48**:434–452.

Otyepka M, Berka K, and Anzenbacher P (2012) Is there a relationship between the substrate preferences and structural flexibility of cytochromes P450? *Curr Drug Metab* **13**:130–142.

Paine MJ, McLaughlin LA, Flanagan JU, Kemp CA, Sutcliffe MJ, Roberts GC, and Wolf CR (2003) Residues glutamate 216 and aspartate 301 are key determinants of substrate specificity and product regioselectivity in cytochrome P450 2D6. *J Biol Chem* **278**:4021–4027.

Rendic S and Guengerich FP (2015) Survey of human oxidoreductases and cytochrome P450 enzymes involved in the metabolism of xenobiotic and natural chemicals. *Chem Res Toxicol* **28**: 38–42.

Rowland P, Blaney FE, Smyth MG, Jones JJ, Leydon VR, Oxbrow AK, Lewis CJ, Tennant MG, Modi S, Eggleston DS, et al. (2006) Crystal structure of human cytochrome P450 2D6. *J Biol Chem* **281**:7614–7622.

Shah MB, Liu J, Huo L, Zhang Q, Dearing MD, Wilderman PR, Szklarz GD, Stout CD, and Halpert JR (2016) Structure-function analysis of mammalian CYP2B enzymes using 7-substituted coumarin derivatives as probes: utility of crystal structures and molecular modeling in understanding xenobiotic metabolism. *Mol Pharmacol* **89**:435–445.

Shah MB, Wilderman PR, Liu J, Jang HH, Zhang Q, Stout CD, and Halpert JR (2015) Structural and biophysical characterization of human cytochromes P450 2B6 and 2A6 bound to volatile hydrocarbons: analysis and comparison. *Mol Pharmacol* **87**:649–659.

Shah MB, Wilderman PR, Pascual J, Zhang Q, Stout CD, and Halpert JR (2012) Conformational adaptation of human cytochrome P450 2B6 and rabbit cytochrome P450 2B4 revealed upon binding multiple amlodipine molecules. *Biochemistry* **51**:7225–7238.

Shen Z, Cheng F, Xu Y, Fu J, Xiao W, Shen J, Liu G, Li W, and Tang Y (2012) Investigation of indazole unbinding pathways in CYP2E1 by molecular dynamics simulations. *PLoS One* **7**:e33500.

Skopalík J, Anzenbacher P, and Otyepka M (2008) Flexibility of human cytochromes P450: molecular dynamics reveals differences between CYPs 3A4, 2C9, and 2A6, which correlate with their substrate preferences. *J Phys Chem B* **112**:8165–8173.

Urban P, Lautier T, Pompon D, and Truan G (2018) Ligand access channels in cytochrome P450 enzymes: a review. *Int J Mol Sci* **19**:1617.

Urban P, Truan G, and Pompon D (2015) Access channels to the buried active site control substrate specificity in CYP1A P450 enzymes. *Biochim Biophys Acta* **1850**:696–707.

Wade RC, Winn PJ, Schlichting I, and Sudarko (2004) A survey of active site access channels in cytochromes P450. *J Inorg Biochem* **98**:1175–1182.

Wang A, Savas U, Hsu MH, Stout CD, and Johnson EF (2012) Crystal structure of human cytochrome P450 2D6 with prinomastat bound. *J Biol Chem* **287**:10834–10843.

Wang A, Stout CD, Zhang Q, and Johnson EF (2015) Contributions of ionic interactions and protein dynamics to cytochrome P450 2D6 (CYP2D6) substrate and inhibitor binding. *J Biol Chem* **290**:5092–5104.

Winn PJ, Lüdemann SK, Gauges R, Lounnas V, and Wade RC (2002) Comparison of the dynamics of substrate access channels in three cytochrome P450s reveals different opening mechanisms and a novel functional role for a buried arginine. *Proc Natl Acad Sci USA* **99**:5361–5366.

Xin J, Yuan M, Peng Y, and Wang J (2020) Analysis of the deleterious single-nucleotide polymorphisms associated with antidepressant efficacy in major depressive disorder. *Front Psychiatry* **11**:151.

Yu X, Cojocaru V, and Wade RC (2013) Conformational diversity and ligand tunnels of mammalian cytochrome P450s. *Biotechnol Appl Biochem* **60**:134–145.

Yu X, Nandekar P, Mustafa G, Cojocaru V, Lepesheva GI, and Wade RC (2016) Ligand tunnels in T. brucei and human CYP51: insights for parasite-specific drug design. *Biochim Biophys Acta* **1860**:67–78.

Zawaira A, Coulson L, Gallotta M, Karimanzira O, and Blackburn J (2011) On the deduction and analysis of singlet and two-state gating-models from the static structures of mammalian CYP450. *J Struct Biol* **173**:282–293.

Zhao Y, White MA, Muralidhara BK, Sun L, Halpert JR, and Stout CD (2006) Structure of microsomal cytochrome P450 2B4 complexed with the antifungal drug bifonazole: insight into P450 conformational plasticity and membrane interaction. *J Biol Chem* **281**:5973–5981.</jrn >

Address correspondence to: Laura Lowe Furge, Department of Chemistry, Kalamazoo College, 1200 Academy Street, Kalamazoo, MI 49006. E-mail: Laura.Furge@kzoo.edu